

## Primordial black holes and scalar-induced gravitational waves from the polynomial attractor model

Zhongkai Wang (王中凯)<sup>1,‡</sup> Shengqing Gao (高盛晴)<sup>1,†</sup> Yungui Gong (龚云贵)<sup>1,2,\*</sup> and Yue Wang (王岳)<sup>1,§</sup>

<sup>1</sup>*School of Physics, Huazhong University of Science and Technology, Wuhan, Hubei 430074, China*

<sup>2</sup>*Department of Physics, School of Physical Science and Technology, Ningbo University, Ningbo, Zhejiang 315211, China*



(Received 5 February 2024; accepted 2 May 2024; published 20 May 2024)

Primordial black holes (PBHs) generated in the early Universe are considered as one of the candidates for dark matter. To produce PBHs with sufficient abundance, the primordial scalar power spectrum needs to be enhanced to the order of 0.01. Considering the third-order polynomial potential with polynomial attractors, we show that PBHs with a mass of about  $10^{17}$  g can be produced while satisfying the constraints from the cosmic microwave background observations at the  $2\sigma$  confidence level. The mass of PBHs produced in the polynomial attractors can be much bigger than that in the exponential  $\alpha$  attractors. By adding a negative power-law term to the polynomials, abundant PBHs with different masses and the accompanying scalar-induced gravitational waves (SIGWs) with different peak frequencies are easily generated. The PBHs with masses around  $10^{-15}$ – $10^{-12}M_{\odot}$  can account for almost all dark matter. The SIGWs generated in the nanohertz band can explain the recent detection of stochastic gravitational-wave background by the pulsar timing array observations. The non-Gaussianities of the primordial curvature perturbations in the squeezed and equilateral limits are calculated numerically. We find that the non-Gaussianity correction enhances the PBH abundance which makes the production of PBHs much easier, but the effect of non-Gaussianity on the generation of SIGWs is negligible.

DOI: [10.1103/PhysRevD.109.103532](https://doi.org/10.1103/PhysRevD.109.103532)

### I. INTRODUCTION

The direct detection of gravitational waves (GWs) by the Laser Interferometer Gravitational-Wave Observatory (LIGO) and Virgo Collaborations opened a new window to test gravity and understand the Universe [1–6]. In particular, some of the binary black holes observed may consist of primordial black holes (PBHs) [7–12], and the detections of stochastic GW background by pulsar timing arrays (PTAs) also hint at the existence of PBHs [13–25]. Furthermore, PBHs can be regarded as one of the candidates for dark matter (DM) and their abundance and mass ranges are tightly constrained by observations [26–31].

If overdense inhomogeneities seeded from the primordial curvature perturbations at the horizon reentry exceed the threshold value  $\delta_c$  during radiation domination, then PBHs could form in the overdense regions through gravitational collapse [32–34]. Accompanied by the generation of PBHs, the large curvature perturbation also produces scalar-induced GWs (SIGWs) that contribute to the stochastic gravitational-wave background (SGWB) [35–45].

To generate a significant abundance of PBHs, the amplitude of the power spectrum  $\mathcal{P}_{\zeta}$  of the primordial curvature perturbation  $\zeta$  should be  $A_s \sim \mathcal{O}(0.01)$  at small scales [46–70]. Compared with the constraint on the amplitude of the power spectrum at the cosmic microwave background (CMB) scales  $A_s \approx 2.1 \times 10^{-9}$  [71], the power spectrum at small scales has to be enhanced by at least 7 orders of magnitude.

To amplify the power spectrum at small scales, a straightforward way is to construct a flat plateau, i.e., an inflection point in the canonical inflation potential [62–70,72–80], leading to the so-called ultraslow-roll (USR) [81,82] stage during inflation. From the fact that an  $m$ -order polynomial has  $m - 2$  inflection points, the potential with  $m = 3$  can have one inflection point in the inflaton potential. Thus, there are some attempts to combine the exponential  $\alpha$  attractor models [83–92] with the third-order polynomial  $V(\psi) = V_0[1 + c_1 f(\psi) + c_2 f^2(\psi) + c_3 f^3(\psi)]^2$  to amplify the power spectrum and generate abundant PBHs [80,93–95]. However, the masses of PBHs produced from these models are too small. Adding a negative power-law term  $f^{-2}(\psi)$  can solve this problem [95].

Apart from the exponential  $\alpha$  attractors, there are also polynomial  $\alpha$  attractors [92,96–99]. Extending the polynomial  $\alpha$  attractors to a hybrid polynomial attractor model, the possibility of PBH production and SGWB generation

\*Corresponding author: ygong@hust.edu.cn

†gaoshengqing@hust.edu.cn

‡ztl@hust.edu.cn

§ywang123@hust.edu.cn

was studied with a two-stage inflation [100]. In this paper, we replace the exponential  $\alpha$  attractors with the polynomial  $\alpha$  attractors in the third-order polynomial potential with and without the additional negative power-law term.

Near the inflection point, the slow-roll (SR) conditions are violated [74] and there may exist a non-negligible non-Gaussianity. The abundance of PBHs and the energy density of accompany SIGWs can be affected by large non-Gaussianity of the primordial curvature perturbations [101–110]. The impacts of non-Gaussianity of the primordial curvature perturbation  $\zeta$  on the formation of PBHs were discussed in the literature [111–117]. There are some methods to calculate the PBH fractional energy density  $\beta$  in the presence of non-Gaussianity, such as changing the variables in the Gaussian probability density function [118] and adopting the path-integral formulation [101,102]. In this paper, we use the latter method to calculate  $\beta$ .

This paper is organized as follows. In Sec. II, we show the models in detail and present the power spectra of the models. In Sec. III, we discuss the PBH abundance produced from the models. In Sec. IV, we compute the generation of SIGWs during radiation domination. We also compare the SIGWs produced in the models with the recent detection of nanohertz stochastic GW background by the North American Nanohertz Observatory for Gravitational Waves (NANOGrav) [119] and the European Pulsar Timing Array (EPTA) [120]. In Sec. V, we calculate the non-Gaussianities of one model in the squeezed and equilateral limits and discuss the effects of non-Gaussianity on the production of PBHs and SIGWs. We conclude the paper in Sec. VI.

## II. THE MODELS

For the enhancement of the primordial scalar power spectrum at small scales with  $\alpha$  attractors, third-order polynomial potentials with an inflection point

$$V(\psi) = V_0[1 + c_1 f(\psi) + c_2 f^2(\psi) + c_3 f^3(\psi)]^2 \quad (1)$$

were usually discussed [80,93–95]. For T models,  $f = f_t(\psi) = \tanh(\psi/\sqrt{6\alpha})$  [80,93]; for E models,  $f = f_e(\psi) = \exp(-\sqrt{2/3}\alpha\psi)$  [94], this also belongs to exponential  $\alpha$  attractors [92]. The masses of PBHs produced by T models with the potential (1) are smaller than  $10^8$  g [93], and the PBHs produced by E models with the potential (1) are asteroid-sized black holes [94]. To obtain PBHs with larger masses, one must decrease the spectral tilt  $n_s$  [95]. Because of the observational constraint by Planck observations,  $n_s = 0.9649 \pm 0.0042$  (68% confidence level) [71], the spectral tilt  $n_s$  cannot decrease too much. To overcome this problem, a negative power-law term  $f^{-2}(\psi)$  was added to the potential for E models with extreme fine-tuning of the parameters [95].

On the other hand, the polynomial potential with inverse powers

$$V(\psi) = V_0 \left( 1 - \frac{\mu^k}{\psi^k} + \dots \right) \quad (2)$$

gives the polynomial  $\alpha$  attractors [92]

$$n_s = 1 - \frac{2k+1}{Nk+2}, \quad r = \frac{(4k)^{\frac{2}{k+2}}(3\alpha)^{\frac{k}{k+2}}}{[(k/2+1)N]^{2-\frac{2}{k+2}}}, \quad (3)$$

where  $N$  is the total number of e-folds before the end of inflation when the pivotal scale  $k_*$  exits the horizon, and  $r$  is the tensor-to-scalar ratio,  $\alpha = 2\mu^2/3$ .

In this paper, we use the polynomial attractor [92] to discuss the enhancement of the primordial scalar power spectrum at small scales from the polynomial potential (1) with the addition of one negative power-law term,

$$V(\psi) = V_0[1 + c_4 f_n^{-1}(\psi) + c_1 f_n(\psi) + c_2 f_n^2(\psi) + c_3 f_n^3(\psi)]^2, \quad (4)$$

where the function  $f_n(\psi) = \psi^{-n}$  and we choose  $n = 3$  for the discussion of PBH production and SGWB generation. The factor  $(k+1)/(k+2)$  in Eq. (3) helps to increase the value of  $n_s$ , so the usual SR stage can be shorter and it is possible to get larger mass PBHs with the polynomial  $\alpha$  attractors than with T and E models. To understand why the model works and how to choose the model parameters, we divide the total number of e-folds  $N$  into two parts, the first part is the SR stage with the number of e-folds  $N_{\text{sr}}$ , the second part is the USR stage until the end of inflation with the number of e-folds  $N - N_{\text{sr}}$ . Since the polynomial attractors (3) are obtained for SR inflation, in the discussion of observational constraints by Planck, we should use  $N_{\text{sr}}$  in Eq. (3); then we use the result to guide us to choose model parameters. Note that the division into SR and USR stages is not exact and is just a rough approximation, so the attractors (3) determined by the SR stage are not the exact predictions of the model, and the results for  $n_s$  and  $r$  are actually obtained by numerical calculation.

For the potential (1), the inflection point (IP) is

$$f(\psi^{\text{IP}}) = -\frac{c_2}{3c_3}, \quad (5)$$

and the derivative of the potential  $V(f(\psi))$  at the inflection point is

$$V'(f(\psi^{\text{IP}})) = c_1 - \frac{c_2^2}{3c_3}. \quad (6)$$

If we choose the value of  $c_1$  so that the derivative of the potential at the inflection point  $\psi^{\text{IP}}$  is exactly zero, then usually we will get a very large number of e-folds. To avoid

a big number of e-folds  $N$ , we add a small number  $\delta$  to  $c_1$  so that the derivative of the potential at the inflection point  $\psi^{\text{IP}}$  is close to zero, but not exactly zero, i.e., we introduce  $\delta$  to adjust the value of  $N$ ,

$$c_1 = \frac{c_2^2}{3c_3} + \delta, \quad \delta \ll 1. \quad (7)$$

To compare the enhancement of the power spectrum between exponential  $\alpha$  attractors and polynomial  $\alpha$  attractors, we first discuss the difference between the results for the potential (1) with  $f = f_e$  and  $f = f_n$ , then we will discuss the power spectrum of the polynomial  $\alpha$  attractor with the potential (4).

### A. Exponential and polynomial attractors

There are three parameters in the polynomial potential (1). The condition (6) for the inflection point reduces one parameter, so there are two free parameters left. At large  $\psi$ , the potential (1) is dominated by the linear term  $c_1 f(\psi)$  and the results depend on the parameter  $c_1$  only because of the existence of attractors. The value of  $V_0$  is determined by the amplitude of the scalar power spectrum.

To show how to determine the model parameters, we take the model  $f(\psi) = f_2 = \psi^{-2}$  as an example. Even though the attractors (3) are independent of  $c_1$ , the value of the scalar field  $\psi_*$  at the pivot scale  $k_* = 0.05 \text{ Mpc}^{-1}$  is  $\psi_* \approx (-16c_1 N_{\text{sr}})^{1/4}$ , so  $\psi_*$  is determined by  $c_1$  and the e-folds  $N_{\text{sr}}$  for the SR stage. Because of the attractors (3) and the CMB constraints on  $n_s$  and  $r$ ,  $N_{\text{sr}}$  cannot be too small. In order to enhance the power spectrum at small scales,  $N_{\text{sr}}$  cannot be too large either. For the convenience of discussion on the choices of parameters and the rough estimation of the observables at large scales, we take a fiducial  $N_{\text{sr}} = 40$ . Note that the actual value of  $N_{\text{sr}}$  is obtained by numerical calculation and is different for different models and model parameters. For fixed  $N_{\text{sr}}$ ,  $\psi_*$  is determined by  $c_1$ . The value of  $\psi_*$  is larger if  $|c_1|$  is larger. Once we take a value of  $c_1$ , then  $c_2$  and  $\psi^{\text{IP}}$  can be determined from  $c_1$  and  $c_3$ . Combining Eqs. (5) and (7), we get  $\psi^{\text{IP}} = (3c_3/c_1)^{1/4} = 2(-3c_3 N_{\text{sr}})^{1/4}/\psi_*$ , so  $\psi^{\text{IP}}$  is smaller if  $|c_1|$  is larger. Now we fix  $c_3 = -1.2$  and  $N_{\text{sr}} = 40$  to get  $\psi_*$  by choosing  $c_1 = -1.7, -1.9, -2.1$ , respectively, then we adjust the value of  $\delta$  and numerically solve the background and perturbed cosmological equations to

obtain the scalar power spectrum  $\mathcal{P}_\zeta$  of the primordial curvature perturbation  $\zeta$ , the scalar spectral tilt  $n_s$ , and the tensor-to-scalar ratio  $r$  at the pivot scale  $k_*$ . The results show that, as  $|c_1|$  becomes larger,  $\psi_*$  and  $r$  are bigger, but  $N$  and  $k^{\text{peak}}$  become smaller. For bigger  $|c_1|$ , the power spectrum can be enhanced to the order of 0.01 with a smaller number of e-folds, so the scale at the end of inflation is also smaller, which leads to a smaller peak scale  $k^{\text{peak}}$  even though  $\psi^{\text{IP}}$  is smaller. Therefore, to get massive PBHs, we should take the bigger value of  $|c_1|$ . However, if  $|c_1|$  is too large, then inflation ends before the inflection point and the enhancement cannot happen. On the other hand, if  $|c_1|$  is too small, then the inflaton stays at the inflection point for a much longer time, leading to a large number of  $N$ . Since  $N$  becomes smaller for larger  $|c_1|$ , we can increase  $N_{\text{sr}}$  to get bigger  $n_s$ . Even though we get bigger  $n_s$  and smaller  $r$ , the peak scale  $k^{\text{peak}}$  becomes larger and the mass of generated PBHs becomes smaller, so we still use smaller  $N_{\text{sr}}$ .

Now we fix  $c_1 = -2.1$  and  $\psi_* = 6.055$ , then vary the value of  $c_3$ . The results tell us that  $N$ ,  $n_s$ , and  $k^{\text{peak}}$  are smaller with smaller  $|c_3|$ . Again, if we increase  $\psi_*$  to get larger  $n_s$  for the same  $c_3$ ,  $k^{\text{peak}}$  becomes bigger. The above discussion tells us that we need to choose larger  $|c_1|$  and smaller  $|c_3|$  to get smaller  $k^{\text{peak}}$ .

To make a comparison for the models  $f_e$  and  $f_n$  with different  $n$ , we fix  $n_s = 0.9565$ , which is consistent with the Planck constraint at the  $2\sigma$  confidence level. Following the procedure discussed above, we can find the appropriate parameters for each model, then we calculate the power spectra, and the results are shown in Table I. Even though we take the lower limit of the  $2\sigma$  confidence level of the Planck results,  $k^{\text{peak}}$  can only be as small as  $10^{14} - 10^{15} \text{ Mpc}^{-1}$  for the models  $f_n$ , and  $k^{\text{peak}}$  is about  $10^{18} \text{ Mpc}^{-1}$  for the model  $f_e$ . Furthermore, for the polynomial attractors  $f_n$ ,  $N$  is smaller than 40. If we increase  $\psi_*$ ,  $N$  and  $n_s$  can be bigger, but then  $k^{\text{peak}}$  becomes bigger too. On the other hand, the results in Table I show that  $k^{\text{peak}}$  in the model  $f_n$  can be smaller than that in the model  $f_e$ , so we only consider the polynomial attractor  $f_3$  in the following discussions.

### B. Modified polynomial attractors

As discussed above, it is very difficult to produce bigger PBHs with the third-order polynomial potentials (1), so we consider the modified polynomial potential (4). We choose

TABLE I. The parameters and results of different models. The unit of  $k^{\text{peak}}$  is  $\text{Mpc}^{-1}$ .

Models	$V_0$	$c_1$	$c_3$	$\delta$	$\psi_*$	$N$	$r$	$\mathcal{P}_\zeta^{\text{peak}}$	$k^{\text{peak}}$
$f_1$	$3.3 \times 10^{-9}$	-2.9	-1.16	$2.84193 \times 10^{-2}$	8.787	39.4	0.0503	0.011	$2.8 \times 10^{14}$
$f_2$	$5.5 \times 10^{-10}$	-2.5	-1.16	$8.48823 \times 10^{-2}$	6.113	37.8	0.0147	0.01	$4.3 \times 10^{14}$
$f_3$	$1.8 \times 10^{-10}$	-2.2	-1.17	$1.284273 \times 10^{-1}$	4.729	38.8	0.0053	0.014	$1.6 \times 10^{15}$
$f_e$	$1.25 \times 10^{-10}$	-2.6	-1.15	$3.74916 \times 10^{-2}$	5.461	51.1	0.0037	0.010	$7.2 \times 10^{18}$

TABLE II. The parameters and results of modified polynomial attractors. The unit of  $k^{\text{peak}}$  is  $\text{Mpc}^{-1}$ .

Models	$V_0$	$\delta$	$c_1$	$c_4$	$\psi_*$	$N$	$n_s$	$\alpha_s$	$r$	$\mathcal{P}_\zeta^{\text{peak}}$	$k^{\text{peak}}$
A1	$8.33 \times 10^{-10}$	$1.1007 \times 10^{-3}$	-1.07	$3.2 \times 10^{-4}$	3.75	63.2	0.9658	-0.0041	0.025	0.0338	$3.0 \times 10^8$
A2	$3.53 \times 10^{-10}$	$6.3843 \times 10^{-4}$	-1.1	$1.3 \times 10^{-4}$	4.0	54.8	0.9652	-0.0015	0.011	0.029	$1.7 \times 10^{12}$
A3	$2.75 \times 10^{-10}$	$7.574 \times 10^{-4}$	-1.12	$9.5 \times 10^{-5}$	4.08	52.4	0.9655	-0.0017	0.008	0.0269	$3.6 \times 10^{13}$

three sets of parameters for the model  $f_3$  and denote them as A1, A2, and A3, respectively.

We take  $c_3 = -1.2$  for the models A1, A2, and A3, and the values of the other parameters are shown in Table II. Note that the  $c_4$  term will affect the inflection point (5) and the relation (7), but its effect is very small near the inflection point, so we still use Eq. (7) to determine  $c_2$  and absorb the effect of  $c_4$  term into  $\delta$ . We plot the potentials of the models and the evolution of the scalar field  $\psi$  in terms of the number of e-folds  $\tilde{N}$  since the pivotal scale  $k_*$  exits the horizon in Fig. 1. From Fig. 1, we see that the inflaton stays at the inflection point for about 15–40 e-folds. The scalar power spectra are shown in Fig. 2. From Fig. 2, we see that the power spectrum for model A1 is broad and the power spectra for models A2 and A3 are narrow. The results for the total number of e-folds  $N$ , the

scalar spectral tilt  $n_s$ , the running of the scalar spectral tilt  $\alpha_s$ , the tensor-to-scalar ratio  $r$ , the peak value of the power spectra  $\mathcal{P}_\zeta^{\text{peak}}$ , and the peak scale  $k^{\text{peak}}$  are also shown in Table II. From Table II, we see that  $n_s$ ,  $r$ , and  $\alpha_s$  are consistent with the recent CMB constraints [71], and the peak scales  $k^{\text{peak}}$  are much smaller compared with those in Table I. In the model A1, we even get  $k^{\text{peak}} = 3 \times 10^8 \text{ Mpc}^{-1}$ . As the peak scale  $k^{\text{peak}}$  becomes smaller, the tensor-to-scalar ratio  $r$  becomes larger, and  $r$  reaches 0.025 in the model A1, so the peak scale  $k^{\text{peak}}$  cannot be very small while satisfying the CMB constraints. As tighter constraints on  $r$  and  $\alpha_s$  are expected in the future CMB observations such as CMB-S4 [121] and LiteBIRD [122], the allowed lower value of the peak scale  $k^{\text{peak}}$  will be limited by future data.

### III. PBH FORMATION

The overdense region generated by large primordial curvature perturbations at small scales may form PBHs through gravitational collapse after the horizon reentry during radiation domination. The mass  $M$  of generated PBHs is of the same order as the horizon mass  $M_H = (2GH)^{-1}$ ,  $M = \gamma M_H$ , where we choose  $\gamma = 0.2$  [32]. Given a scale  $k$ , the PBH mass  $M$  is [30,54]

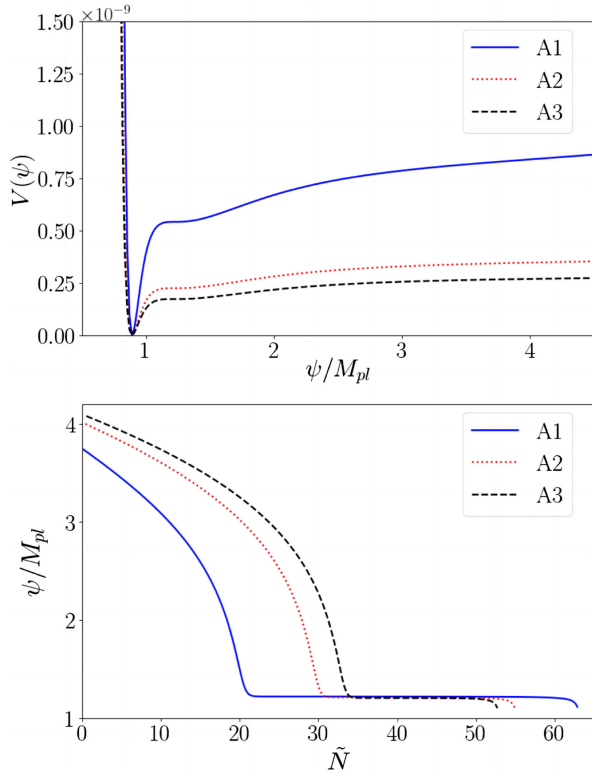


FIG. 1. Upper: potentials of the models A1, A2, and A3. Lower: evolution of the scalar field  $\psi$  in terms of the number of e-folds  $\tilde{N}$  since the pivotal scale  $k_*$  exits the horizon in these models. Blue solid line, model A1; red dotted line, model A2; black dashed line, model A3.

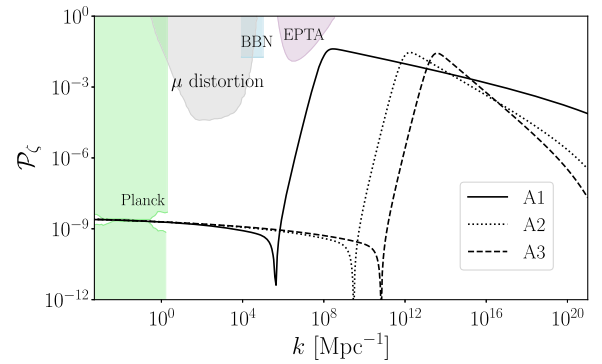


FIG. 2. The results of the power spectra for the models A1, A2, and A3. Black solid line, model A1; black dotted line, model A2; black dashed line, model A3. The light green shaded region is excluded by the CMB observations [71]. The light purple, cyan, and gray regions show the constraints from the PTA observations [123], the effect on the ratio between neutron and proton during the big bang nucleosynthesis (BBN) [124], and  $\mu$ -distortion of CMB [125], respectively.

$$M(k) = 3.68 \left( \frac{\gamma}{0.2} \right) \left( \frac{g_*}{10.75} \right)^{-1/6} \left( \frac{k}{10^6 \text{ Mpc}^{-1}} \right)^{-2} M_\odot, \quad (8)$$

where  $M_\odot$  is the solar mass,  $g_*$  is the effective degrees of freedom at the PBH formation, and we do not distinguish the effective degrees of freedom in the entropy and energy density. The current fractional energy density of PBHs with mass  $M$  to DM is [62]

$$f_{\text{pbh}}(M) = \frac{\beta(M)}{3.94 \times 10^{-9}} \left( \frac{\gamma}{0.2} \right)^{1/2} \left( \frac{g_*}{10.75} \right)^{-1/4} \times \left( \frac{0.12}{\Omega_{\text{DM}} h^2} \right) \left( \frac{M}{M_\odot} \right)^{-1/2}, \quad (9)$$

where  $\Omega_{\text{DM}}$  is the current energy density of DM, and the Hubble constant  $H_0 = 100h$  km/s/Mpc. The PBH fractional energy density  $\beta(M)$  at the formation for Gaussian curvature perturbation  $\zeta$  is [126]

$$\beta^G(M) \approx \sqrt{\frac{2}{\pi}} \frac{\sigma_R(M)}{\delta_c} \exp\left(-\frac{\delta_c^2}{2\sigma_R^2(M)}\right), \quad (10)$$

where  $\delta_c$  is the critical density perturbation for the PBH formation. The mass variance  $\sigma_R(k)$  on the comoving scale  $k = aH = R^{-1}$  is [126]

$$\sigma_R^2(k) = \left( \frac{4}{9} \right)^2 \int \frac{dq}{q} W^2(q/k) (q/k)^4 \mathcal{P}_\zeta(q), \quad (11)$$

and the Gaussian window function  $W(x) = \exp(-x^2/2)$ . In this paper, we choose the parameters as  $\delta_c = 0.4$  [127–131],  $g_* = 106.75$ , and  $\Omega_{\text{DM}} h^2 = 0.12$ . Using the power spectra

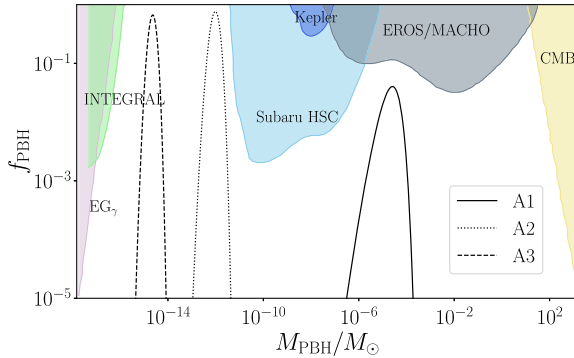


FIG. 3. The abundance of PBHs produced by the models A1, A2, and A3. Black solid line, model A1; black dotted line, model A2; black dashed line, model A3. The shaded regions are the observational constraints on PBH abundance: the light purple region from extragalactic  $\gamma$  rays by PBH evaporation (EG $\gamma$ ) [132], the green region from the Galactic Center 511 keV  $\gamma$ -ray line (INTEGRAL) [133], the cyan region from microlensing events with Subaru HSC [134], the deep blue region from the Kepler satellite [135], the gray region from the EROS/MACHO [136], and the khaki region from accretion constraints by CMB [137].

TABLE III. The results for the abundance and peak mass of PBHs and the peak frequency of SIGWs for the models A1, A2, and A3.

Models	$M^{\text{peak}}/M_\odot$	$f_{\text{pbh}}$	$f_c/\text{Hz}$
A1	$2.51 \times 10^{-5}$	0.04	$5.56 \times 10^{-7}$
A2	$9.99 \times 10^{-13}$	0.765	$3.13 \times 10^{-3}$
A3	$2.29 \times 10^{-15}$	0.669	$6.44 \times 10^{-2}$

given in Fig. 2, we numerically compute the abundance of PBHs with the above formulas and the results for the models A1, A2, and A3 are shown in Fig. 3. The results show that all the produced PBHs satisfy the observational constraints. The peak values of the mass and the abundance of PBH produced at the peak scale  $k^{\text{peak}}$  are shown in Table III. As seen from Table III, in the models A1, A2, and A3, the PBH masses are around  $10^{-5}M_\odot$ ,  $10^{-12}M_\odot$ , and  $10^{-15}M_\odot$ , respectively. PBHs with masses around  $10^{-12}M_\odot$  and  $10^{-15}M_\odot$  can account for most of DM.

#### IV. SCALAR-INDUCED GRAVITATIONAL WAVES

Accompanied by the production of PBHs, the large primordial curvature perturbations at small scales can source the tensor perturbation at the second order after the horizon reentry to generate SIGWs. In this section, we calculate the energy density of SIGWs generated in the models A1, A2, and A3.

The second-order tensor perturbation expressed in terms of the Fourier components is

$$h_{ij}(\mathbf{x}, \eta) = \int \frac{d^3\mathbf{k}}{(2\pi)^{3/2}} e^{i\mathbf{k}\cdot\mathbf{x}} [h_{\mathbf{k}}(\eta) e_{ij}(\mathbf{k}) + \bar{h}_{\mathbf{k}}(\eta) \bar{e}_{ij}(\mathbf{k})], \quad (12)$$

where  $e_{ij}(\mathbf{k})$  and  $\bar{e}_{ij}(\mathbf{k})$  are the plus and cross polarization tensors. The power spectrum of the SIGWs is

$$\langle h_{\mathbf{k}}(\eta) h_{\mathbf{q}}(\eta) \rangle = \frac{2\pi^2}{k^3} \delta^{(3)}(\mathbf{k} + \mathbf{q}) \mathcal{P}_h(k, \eta). \quad (13)$$

The fractional energy density of SIGWs is [39]

$$\Omega_{\text{GW}}(k) = \frac{1}{24} \left( \frac{k}{\mathcal{H}} \right)^2 \overline{\mathcal{P}_h(k, \eta)}. \quad (14)$$

Since GWs behave like radiation, the current fractional energy density of SIGWs is

$$\Omega_{\text{GW}0}(k) = \Omega_{\text{GW}}(k) \frac{\Omega_{r0}}{\Omega_r(\eta)}, \quad (15)$$

where  $\Omega_r(\eta)$  is the fraction energy density of radiation and  $\Omega_{r0}$  is its current value.

Using the power spectra given in Fig. 2, we calculate  $\Omega_{\text{GW}0}$  for the models A1, A2, and A3 and the results are

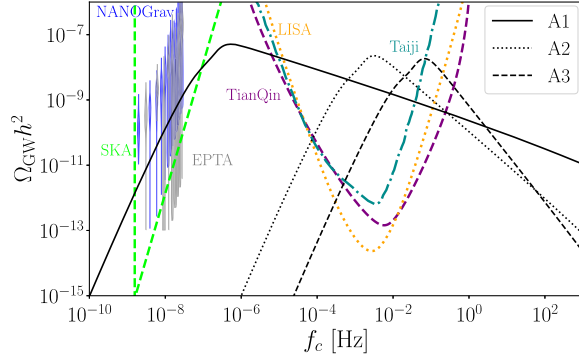


FIG. 4. The SIGWs generated from the models A1, A2, and A3. Black solid line, model A1; black dotted line, model A2; black dashed line, model A3. The blue and gray violins represent the NANOGrav 15-yr and EPTA DR2 data, respectively [119,120]. The green dashed curve denotes the SKA limit [138]. The purple dashed curve denotes the TianQin limit [139], the orange dotted curve denotes the LISA limit [140], and the cyan dot-dashed curve denotes the Taiji limit [141]. The limits set by SKA, TianQin, LISA, and Taiji are the expected sensitivities when they are in operation in the future.

shown in Fig. 4. The value of the peak frequency  $f_c$  where  $\Omega_{\text{GW}0}$  takes the maximum value is shown in Table III. For the model A1, even though the peak frequency of the SIGWs is around  $10^{-7}$  Hz, the SIGWs have a broad spectrum and they can be detected in both the nano- and millihertz frequency bands. The infrared parts of the SIGWs in the model A1 are consistent with the stochastic GW background detected by NANOGrav and EPTA. For the models A2 and A3, the spectra of the SIGWs are relatively narrow. The peak frequency of SIGWs for the model A2 is around  $10^{-3}$  Hz and the peak frequency of SIGWs for the model A3 is around  $10^{-2}$  Hz. The SIGWs for the models A2 and A3 can be tested by future spaceborne GW detectors such as TianQin, Taiji, and LISA.

## V. PRIMORDIAL NON-GAUSSIANITY

In this section, we calculate the non-Gaussianity of the primordial curvature perturbation  $\hat{\zeta}$  by taking the model A1 as an example. From the definition of the bispectrum  $B_\zeta$  [142,143]

$$\langle \hat{\zeta}_{k_1} \hat{\zeta}_{k_2} \hat{\zeta}_{k_3} \rangle = (2\pi)^3 \delta^{(3)}(\mathbf{k}_1 + \mathbf{k}_2 + \mathbf{k}_3) B_\zeta(k_1, k_2, k_3), \quad (16)$$

we get the non-Gaussianity parameter  $f_{\text{NL}}$  [142]

$$f_{\text{NL}}(k_1, k_2, k_3) = \frac{5}{6} \frac{B_\zeta(k_1, k_2, k_3)}{P_\zeta(k_1)P_\zeta(k_2) + P_\zeta(k_1)P_\zeta(k_3) + P_\zeta(k_2)P_\zeta(k_3)}, \quad (17)$$

where  $P_\zeta(k) = 2\pi^2 \mathcal{P}_\zeta(k)/k^3$ , and the explicit form of the bispectrum  $B_\zeta(k_1, k_2, k_3)$  can be found in [107,144]. In the

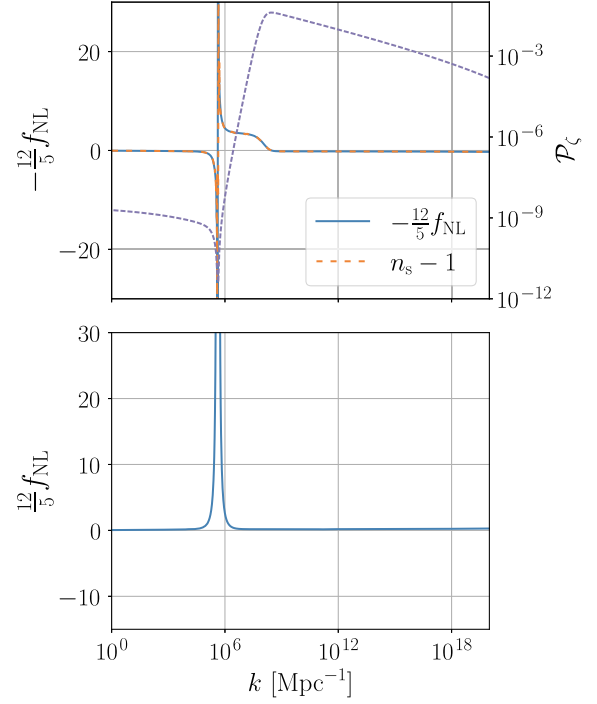


FIG. 5. The primordial scalar power spectrum  $\mathcal{P}_\zeta$  and the non-Gaussianity parameter  $f_{\text{NL}}$  for model A1. Upper: the purple dashed line represents the power spectrum  $\mathcal{P}_\zeta$ , the blue solid line represents  $-\frac{12}{5}f_{\text{NL}}$  in the squeezed limit with  $k_1 = k_2 = 10^6 k_3 = k$ , and the orange dashed line represents the scalar spectral tilt  $n_s - 1$ . Lower:  $\frac{12}{5}f_{\text{NL}}$  in the equilateral limit with  $k_1 = k_2 = k_3 = k$ .

squeezed limit  $k_3 \rightarrow 0$ , there is a consistency relationship between the non-Gaussianity parameter  $f_{\text{NL}}$  and the scalar spectral tilt  $n_s$  [145]

$$\lim_{k_3 \rightarrow 0} f_{\text{NL}}(k_1, k_2, k_3) = \frac{5}{12} (1 - n_s). \quad (18)$$

Although the consistency relation was originally derived in the canonical single-field inflation with slow-roll conditions, it was then proved to be true for any inflation in which the inflaton is the only dynamical field during inflation [146].

For the model A1, we numerically calculate  $f_{\text{NL}}$  in the squeezed and the equilateral limits and the results are shown in Fig. 5. As shown in the upper panel of Fig. 5, the consistency relation holds in the squeezed limit. In this model, the value of  $f_{\text{NL}}$  is small when the power spectrum reaches the peak and is pretty large at scales around  $k \sim 10^6 \text{ Mpc}^{-1}$ . The large values of  $f_{\text{NL}}$  are due to the plunge of the power spectrum by several orders of magnitude. The change of the scalar spectral tilt near the peak is small, so the squeezed limit  $f_{\text{NL}}$  is almost constant when the power spectrum climbs up and rolls down the peak.

Considering the non-Gaussianity of the primordial curvature perturbation  $\zeta$ , the PBH fractional energy density becomes [102,104–106]

$$\beta = e^{\Delta_3} \beta^G. \quad (19)$$

Since the mass of PBHs is almost monochromatic in the model A1, we can consider the correction on the peak scales only, so the third cumulant  $\Delta_3$  can be approximated as [108]

$$\Delta_3 \approx \frac{23\delta_c^3}{\mathcal{P}_\zeta(k^{\text{peak}})} f_{\text{NL}}(k^{\text{peak}}, k^{\text{peak}}, k^{\text{peak}}). \quad (20)$$

In the model A1, we have  $\delta_c = 0.4$ ,  $\mathcal{P}_\zeta(k^{\text{peak}}) = 0.0338$ , and  $f_{\text{NL}}(k^{\text{peak}}, k^{\text{peak}}, k^{\text{peak}}) = 0.0754$ , so the third cumulant  $\Delta_3 = 3.28 > 1$ . Therefore the non-Gaussianity correction enhances the PBH abundance and this correction makes the production of PBHs easier.

In terms of the local-type non-Gaussianity parameter  $f_{\text{NL}}$ , the primordial curvature perturbation can be parametrized as

$$\zeta(\mathbf{x}) = \zeta^G(\mathbf{x}) + \frac{3}{5} f_{\text{NL}} (\zeta^G(\mathbf{x})^2 - \langle \zeta^G(\mathbf{x})^2 \rangle), \quad (21)$$

where  $\zeta^G(\mathbf{x})$  is the Gaussian part of the curvature perturbation. The power spectrum of the curvature perturbation is

$$\mathcal{P}_\zeta(k) = \mathcal{P}_\zeta^G(k) + \mathcal{P}_\zeta^{\text{NG}}(k), \quad (22)$$

where the non-Gaussianity correction to the power spectrum is [103,108]

$$\mathcal{P}_\zeta^{\text{NG}}(k) = \left(\frac{3}{5}\right)^2 \frac{k^3}{2\pi} f_{\text{NL}}^2 \int d^3\mathbf{p} \frac{\mathcal{P}_\zeta^G(p)}{p^3} \frac{\mathcal{P}_\zeta^G(|\mathbf{k}-\mathbf{p}|)}{|\mathbf{k}-\mathbf{p}|^3}. \quad (23)$$

From Eq. (23), we expect that the non-Gaussianity correction to the power spectrum mainly comes from the value of  $\mathcal{P}_\zeta^G$  around the vicinity of  $k^{\text{peak}}$ . Therefore, we use  $f_{\text{NL}}$  in the equilateral limit at  $k^{\text{peak}}$  as an estimator for the amplitude of the local-type non-Gaussianity parameter. Using the results for the scalar power spectrum, we get  $\mathcal{P}_\zeta^{\text{NG}}(k^{\text{peak}}) = 3.19 \times 10^{-6}$ . Since the non-Gaussianity correction  $\mathcal{P}_\zeta^{\text{NG}}(k)$  is negligible, the effect of non-Gaussianity on the generation of SIGWs can be neglected.

## VI. CONCLUSION

Taking advantage of the existence of one inflection point in the third-order polynomial potential and inflationary attractors, it was shown that the primordial scalar power spectrum in the models with the combination of the third-order polynomial and exponential  $\alpha$  attractors can satisfy the CMB constraints at large scales and get enhancement at small scales to produce abundant PBHs and generate detectable SIGWs [94]. For the exponential  $\alpha$  attractors, the peak scale of the power spectrum  $k^{\text{peak}}$  is about  $10^{18} \text{ Mpc}^{-1}$ , and the PBHs produced from these models can reach asteroid size only. To produce PBHs with bigger mass, we combine the third-order polynomial and the polynomial attractor models to amplify the power spectrum at small scales. For the polynomial attractors,  $k^{\text{peak}}$  can be as small as  $10^{14}$ – $10^{15} \text{ Mpc}^{-1}$ , and PBHs with the mass about  $10^{17} \text{ g}$  can be produced. However, the mass of PBHs produced in these models is still too small. By adding a negative power-law term to the polynomials, abundant PBHs with different masses and the accompanying SIGWs with different peak frequencies are generated. For the three models considered in this paper, the peak scales  $k^{\text{peak}}$  are  $3 \times 10^8$ ,  $1.7 \times 10^{12}$ , and  $3.6 \times 10^{13} \text{ Mpc}^{-1}$ , respectively; the peak mass of PBHs are  $2.51 \times 10^{-5} M_\odot$ ,  $9.99 \times 10^{-13} M_\odot$ , and  $2.29 \times 10^{-15} M_\odot$ , respectively; the peak frequency of SIGWs are  $5.56 \times 10^{-7}$ ,  $3.13 \times 10^{-3}$ , and  $6.44 \times 10^{-2} \text{ Hz}$ , respectively. The PBHs with masses around  $10^{-15}$ – $10^{-12} M_\odot$  can account for almost all DM. The power spectrum of primordial curvature perturbations for the model A1 is broad and the power spectra for the models A2 and A3 are narrow, so the SIGWs produced have both broad and narrow spectra. The infrared parts of the SIGWs in the model A1 can explain the stochastic GW background detected by NANOGrav and EPTA. The non-Gaussianities of the primordial curvature perturbations in the squeezed and equilateral limits are calculated. We find that the non-Gaussianity correction enhances the PBH abundance, which makes the production of PBHs much easier, but the effect of non-Gaussianity on the generation of SIGWs is negligible.

## ACKNOWLEDGMENTS

This research is supported in part by the National Key Research and Development Program of China under Grant No. 2020YFC2201504.

- [1] B. P. Abbott *et al.* (LIGO Scientific and Virgo Collaborations), Observation of gravitational waves from a binary black hole merger, *Phys. Rev. Lett.* **116**, 061102 (2016).
- [2] B. P. Abbott *et al.* (LIGO Scientific and Virgo Collaborations), GW150914: The Advanced LIGO detectors in the era of first discoveries, *Phys. Rev. Lett.* **116**, 131103 (2016).
- [3] B. P. Abbott *et al.* (LIGO Scientific and Virgo Collaborations), GWTC-1: A gravitational-wave transient catalog of compact binary mergers observed by LIGO and Virgo during the first and second observing runs, *Phys. Rev. X* **9**, 031040 (2019).
- [4] R. Abbott *et al.* (LIGO Scientific and Virgo Collaborations), GWTC-2: Compact binary coalescences observed by LIGO and LIGO and Virgo during the first half of the third observing run, *Phys. Rev. X* **11**, 021053 (2021).
- [5] R. Abbott *et al.* (LIGO Scientific and Virgo Collaborations), GWTC-2.1: Deep extended catalog of compact binary coalescences observed by LIGO and Virgo during the first half of the third observing run, *Phys. Rev. D* **109**, 022001 (2024).
- [6] R. Abbott *et al.* (KAGRA, VIRGO, and LIGO Scientific Collaborations), GWTC-3: Compact binary coalescences observed by LIGO and Virgo during the second part of the third observing run, *Phys. Rev. X* **13**, 041039 (2023).
- [7] S. Bird, I. Cholis, J. B. Muñoz, Y. Ali-Haïmoud, M. Kamionkowski, E. D. Kovetz, A. Raccanelli, and A. G. Riess, Did LIGO detect dark matter?, *Phys. Rev. Lett.* **116**, 201301 (2016).
- [8] M. Sasaki, T. Suyama, T. Tanaka, and S. Yokoyama, Primordial black hole scenario for the gravitational-wave event GW150914, *Phys. Rev. Lett.* **117**, 061101 (2016); **121**, 059901(E) (2018).
- [9] K. Inomata, M. Kawasaki, K. Mukaida, Y. Tada, and T. T. Yanagida, Inflationary primordial black holes for the LIGO gravitational wave events and pulsar timing array experiments, *Phys. Rev. D* **95**, 123510 (2017).
- [10] V. De Luca, V. Desjacques, G. Franciolini, P. Pani, and A. Riotto, GW190521 mass gap event and the primordial black hole scenario, *Phys. Rev. Lett.* **126**, 051101 (2021).
- [11] V. De Luca, G. Franciolini, P. Pani, and A. Riotto, Bayesian evidence for both astrophysical and primordial black holes: Mapping the GWTC-2 catalog to third-generation detectors, *J. Cosmol. Astropart. Phys.* **05** (2021) 003.
- [12] G. Franciolini, V. Baibhav, V. De Luca, K. K. Y. Ng, K. W. K. Wong, E. Berti, P. Pani, A. Riotto, and S. Vitale, Searching for a subpopulation of primordial black holes in LIGO-Virgo gravitational-wave data, *Phys. Rev. D* **105**, 083526 (2022).
- [13] V. De Luca, G. Franciolini, and A. Riotto, NANOGrav data hints at primordial black holes as dark matter, *Phys. Rev. Lett.* **126**, 041303 (2021).
- [14] V. Vaskonen and H. Veermäe, Did NANOGrav see a signal from primordial black hole formation?, *Phys. Rev. Lett.* **126**, 051303 (2021).
- [15] K. Kohri and T. Terada, Solar-mass primordial black holes explain NANOGrav hint of gravitational waves, *Phys. Lett. B* **813**, 136040 (2021).
- [16] G. Domènech and S. Pi, NANOGrav hints on planet-mass primordial black holes, *Sci. China Phys. Mech. Astron.* **65**, 230411 (2022).
- [17] V. Atal, A. Sanglas, and N. Triantafyllou, NANOGrav signal as mergers of stupendously large primordial black holes, *J. Cosmol. Astropart. Phys.* **06** (2021) 022.
- [18] Z. Yi and Z.-H. Zhu, NANOGrav signal and LIGO-Virgo primordial black holes from the Higgs field, *J. Cosmol. Astropart. Phys.* **05** (2022) 046.
- [19] A. Afzal *et al.* (NANOGrav Collaboration), The NANOGrav 15 yr data set: Search for signals from new physics, *Astrophys. J. Lett.* **951**, L11 (2023).
- [20] J. Antoniadis *et al.* (EPTA Collaboration), The second data release from the European Pulsar Timing Array: V. Implications for massive black holes, dark matter and the early Universe, [arXiv:2306.16227](https://arxiv.org/abs/2306.16227).
- [21] Z. Yi, Q. Gao, Y. Gong, Y. Wang, and F. Zhang, Scalar induced gravitational waves in light of pulsar timing array data, *Sci. China Phys. Mech. Astron.* **66**, 120404 (2023).
- [22] G. Franciolini, A. Junior Iovino, V. Vaskonen, and H. Veermäe, Recent gravitational wave observation by pulsar timing arrays and primordial black holes: The importance of non-Gaussianities, *Phys. Rev. Lett.* **131**, 201401 (2023).
- [23] J. Ellis, M. Fairbairn, G. Franciolini, G. Hütsi, A. Iovino, M. Lewicki, M. Raidal, J. Urrutia, V. Vaskonen, and H. Veermäe, What is the source of the PTA GW signal?, *Phys. Rev. D* **109**, 023522 (2024).
- [24] S. Basilakos, D. V. Nanopoulos, T. Papanikolaou, E. N. Saridakis, and C. Tzerefos, Gravitational wave signatures of no-scale supergravity in NANOGrav and beyond, *Phys. Lett. B* **850**, 138507 (2024).
- [25] S. Basilakos, D. V. Nanopoulos, T. Papanikolaou, E. N. Saridakis, and C. Tzerefos, Induced gravitational waves from flipped SU(5) superstring theory at nHz, *Phys. Lett. B* **849**, 138446 (2024).
- [26] P. Ivanov, P. Naselsky, and I. Novikov, Inflation and primordial black holes as dark matter, *Phys. Rev. D* **50**, 7173 (1994).
- [27] M. Y. Khlopov, S. G. Rubin, and A. S. Sakharov, Primordial structure of massive black hole clusters, *Astropart. Phys.* **23**, 265 (2005).
- [28] P. H. Frampton, M. Kawasaki, F. Takahashi, and T. T. Yanagida, Primordial black holes as all dark matter, *J. Cosmol. Astropart. Phys.* **04** (2010) 023.
- [29] K. M. Belotsky, A. D. Dmitriev, E. A. Esipova, V. A. Gani, A. V. Grobov, M. Y. Khlopov, A. A. Kirillov, S. G. Rubin, and I. V. Svadkovsky, Signatures of primordial black hole dark matter, *Mod. Phys. Lett. A* **29**, 1440005 (2014).
- [30] B. Carr, F. Kuhnel, and M. Sandstad, Primordial black holes as dark matter, *Phys. Rev. D* **94**, 083504 (2016).
- [31] B. Carr and F. Kuhnel, Primordial black holes as dark matter: Recent developments, *Annu. Rev. Nucl. Part. Sci.* **70**, 355 (2020).
- [32] B. J. Carr, The primordial black hole mass spectrum, *Astrophys. J.* **201**, 1 (1975).
- [33] S. Hawking, Gravitationally collapsed objects of very low mass, *Mon. Not. R. Astron. Soc.* **152**, 75 (1971).
- [34] B. J. Carr and S. W. Hawking, Black holes in the early Universe, *Mon. Not. R. Astron. Soc.* **168**, 399 (1974).

- [35] K. N. Ananda, C. Clarkson, and D. Wands, The cosmological gravitational wave background from primordial density perturbations, *Phys. Rev. D* **75**, 123518 (2007).
- [36] D. Baumann, P. J. Steinhardt, K. Takahashi, and K. Ichiki, Gravitational wave spectrum induced by primordial scalar perturbations, *Phys. Rev. D* **76**, 084019 (2007).
- [37] R. Saito and J. Yokoyama, Gravitational wave background as a probe of the primordial black hole abundance, *Phys. Rev. Lett.* **102**, 161101 (2009); **107**, 069901(E) (2011).
- [38] K. Kohri and T. Terada, Semianalytic calculation of gravitational wave spectrum nonlinearly induced from primordial curvature perturbations, *Phys. Rev. D* **97**, 123532 (2018).
- [39] J. R. Espinosa, D. Racco, and A. Riotto, A cosmological signature of the SM Higgs instability: Gravitational waves, *J. Cosmol. Astropart. Phys.* **09** (2018) 012.
- [40] R.-G. Cai, S. Pi, S.-J. Wang, and X.-Y. Yang, Pulsar timing array constraints on the induced gravitational waves, *J. Cosmol. Astropart. Phys.* **10** (2019) 059.
- [41] K. Inomata, K. Kohri, T. Nakama, and T. Terada, Enhancement of gravitational waves induced by scalar perturbations due to a sudden transition from an early matter era to the radiation era, *Phys. Rev. D* **100**, 043532 (2019); **108**, 049901(E) (2023).
- [42] G. Domènech, S. Pi, and M. Sasaki, Induced gravitational waves as a probe of thermal history of the Universe, *J. Cosmol. Astropart. Phys.* **08** (2020) 017.
- [43] M. Braglia, X. Chen, and D. K. Hazra, Probing primordial features with the stochastic gravitational wave background, *J. Cosmol. Astropart. Phys.* **03** (2021) 005.
- [44] Z. Yi, Primordial black holes and scalar-induced gravitational waves from the generalized Brans-Dicke theory, *J. Cosmol. Astropart. Phys.* **03** (2023) 048.
- [45] G. Domènech, Scalar induced gravitational waves review, *Universe* **7**, 398 (2021).
- [46] G. Ballesteros and M. Taoso, Primordial black hole dark matter from single field inflation, *Phys. Rev. D* **97**, 023501 (2018).
- [47] I. Dalianis, S. Karydas, and E. Papantonopoulos, Generalized non-minimal derivative coupling: Application to inflation and primordial black hole production, *J. Cosmol. Astropart. Phys.* **06** (2020) 040.
- [48] G. Sato-Polito, E. D. Kovetz, and M. Kamionkowski, Constraints on the primordial curvature power spectrum from primordial black holes, *Phys. Rev. D* **100**, 063521 (2019).
- [49] Y. Lu, Y. Gong, Z. Yi, and F. Zhang, Constraints on primordial curvature perturbations from primordial black hole dark matter and secondary gravitational waves, *J. Cosmol. Astropart. Phys.* **12** (2019) 031.
- [50] G. Ballesteros, J. Rey, M. Taoso, and A. Urbano, Primordial black holes as dark matter and gravitational waves from single-field polynomial inflation, *J. Cosmol. Astropart. Phys.* **07** (2020) 025.
- [51] C. Fu, P. Wu, and H. Yu, Primordial black holes from inflation with nonminimal derivative coupling, *Phys. Rev. D* **100**, 063532 (2019).
- [52] J. Lin, Q. Gao, Y. Gong, Y. Lu, C. Zhang, and F. Zhang, Primordial black holes and secondary gravitational waves from  $k$  and  $G$  inflation, *Phys. Rev. D* **101**, 103515 (2020).
- [53] Z. Yi, Y. Gong, B. Wang, and Z.-h. Zhu, Primordial black holes and secondary gravitational waves from the Higgs field, *Phys. Rev. D* **103**, 063535 (2021).
- [54] Z. Yi, Q. Gao, Y. Gong, and Z.-h. Zhu, Primordial black holes and scalar-induced secondary gravitational waves from inflationary models with a noncanonical kinetic term, *Phys. Rev. D* **103**, 063534 (2021).
- [55] H. V. Ragavendra, P. Saha, L. Sriramkumar, and J. Silk, Primordial black holes and secondary gravitational waves from ultraslow roll and punctuated inflation, *Phys. Rev. D* **103**, 083510 (2021).
- [56] R. Kawaguchi and S. Tsujikawa, Primordial black holes from Higgs inflation with a Gauss-Bonnet coupling, *Phys. Rev. D* **107**, 063508 (2023).
- [57] Y. Aldabergenov and S. V. Ketov, Primordial black holes from Volkov-Akulov-Starobinsky supergravity, *Fortschr. Phys.* **71**, 2300039 (2023).
- [58] K. Cheung, C. J. Ouseph, and P.-Y. Tseng, NANOGrav signal and PBH from the modified Higgs inflation, [arXiv:2307.08046](https://arxiv.org/abs/2307.08046).
- [59] D. Hooper, A. Ireland, G. Krnjaic, and A. Stebbins, Supermassive primordial black holes from inflation, *J. Cosmol. Astropart. Phys.* **04** (2024) 021.
- [60] T. Papanikolaou, A. Lymperis, S. Lola, and E. N. Saridakis, Primordial black holes and gravitational waves from non-canonical inflation, *J. Cosmol. Astropart. Phys.* **03** (2023) 003.
- [61] K.-i. Kubota, H. Matsui, and T. Terada, Inflationary  $\alpha$ -attractor models with singular derivative of potential, *J. Cosmol. Astropart. Phys.* **07** (2023) 011.
- [62] H. Di and Y. Gong, Primordial black holes and second order gravitational waves from ultra-slow-roll inflation, *J. Cosmol. Astropart. Phys.* **07** (2018) 007.
- [63] J. Garcia-Bellido and E. Ruiz Morales, Primordial black holes from single field models of inflation, *Phys. Dark Universe* **18**, 47 (2017).
- [64] J. M. Ezquiaga, J. Garcia-Bellido, and E. Ruiz Morales, Primordial black hole production in critical Higgs inflation, *Phys. Lett. B* **776**, 345 (2018).
- [65] C. Germani and T. Prokopec, On primordial black holes from an inflection point, *Phys. Dark Universe* **18**, 6 (2017).
- [66] J. R. Espinosa, D. Racco, and A. Riotto, Cosmological signature of the Standard Model Higgs vacuum instability: Primordial black holes as dark matter, *Phys. Rev. Lett.* **120**, 121301 (2018).
- [67] G. Ballesteros, J. Beltran Jimenez, and M. Pieroni, Black hole formation from a general quadratic action for inflationary primordial fluctuations, *J. Cosmol. Astropart. Phys.* **06** (2019) 016.
- [68] T.-J. Gao and Z.-K. Guo, Primordial black hole production in inflationary models of supergravity with a single chiral superfield, *Phys. Rev. D* **98**, 063526 (2018).
- [69] M. Sasaki, T. Suyama, T. Tanaka, and S. Yokoyama, Primordial black holes—perspectives in gravitational wave astronomy, *Classical Quantum Gravity* **35**, 063001 (2018).
- [70] S. Passaglia, W. Hu, and H. Motohashi, Primordial black holes and local non-Gaussianity in canonical inflation, *Phys. Rev. D* **99**, 043536 (2019).

- [71] Y. Akrami *et al.* (Planck Collaboration), Planck 2018 results. X. Constraints on inflation, *Astron. Astrophys.* **641**, A10 (2020).
- [72] J. Martin, H. Motohashi, and T. Suyama, Ultra slow-roll inflation and the non-Gaussianity consistency relation, *Phys. Rev. D* **87**, 023514 (2013).
- [73] H. Motohashi, A. A. Starobinsky, and J. Yokoyama, Inflation with a constant rate of roll, *J. Cosmol. Astropart. Phys.* **09** (2015) 018.
- [74] H. Motohashi and W. Hu, Primordial black holes and slow-roll violation, *Phys. Rev. D* **96**, 063503 (2017).
- [75] F. Bezrukov, M. Pauly, and J. Rubio, On the robustness of the primordial power spectrum in renormalized Higgs inflation, *J. Cosmol. Astropart. Phys.* **02** (2018) 040.
- [76] M. Cicoli, V. A. Diaz, and F. G. Pedro, Primordial black holes from string inflation, *J. Cosmol. Astropart. Phys.* **06** (2018) 034.
- [77] S. Passaglia, W. Hu, and H. Motohashi, Primordial black holes as dark matter through Higgs field criticality, *Phys. Rev. D* **101**, 123523 (2020).
- [78] N. Bhaumik and R. K. Jain, Primordial black holes dark matter from inflection point models of inflation and the effects of reheating, *J. Cosmol. Astropart. Phys.* **01** (2020) 037.
- [79] W.-T. Xu, J. Liu, T.-J. Gao, and Z.-K. Guo, Gravitational waves from double-inflection-point inflation, *Phys. Rev. D* **101**, 023505 (2020).
- [80] I. Dalianis, A. Kehagias, and G. Tringas, Primordial black holes from  $\alpha$ -attractors, *J. Cosmol. Astropart. Phys.* **01** (2019) 037.
- [81] N. C. Tsamis and R. P. Woodard, Improved estimates of cosmological perturbations, *Phys. Rev. D* **69**, 084005 (2004).
- [82] W. H. Kinney, Horizon crossing and inflation with large eta, *Phys. Rev. D* **72**, 023515 (2005).
- [83] A. A. Starobinsky, A new type of isotropic cosmological models without singularity, *Phys. Lett.* **91B**, 99 (1980).
- [84] D. S. Salopek, J. R. Bond, and J. M. Bardeen, Designing density fluctuation spectra in inflation, *Phys. Rev. D* **40**, 1753 (1989).
- [85] R. Kallosh and A. Linde, Universality class in conformal inflation, *J. Cosmol. Astropart. Phys.* **07** (2013) 002.
- [86] R. Kallosh and A. Linde, Superconformal generalizations of the Starobinsky model, *J. Cosmol. Astropart. Phys.* **06** (2013) 028.
- [87] R. Kallosh and A. Linde, Non-minimal inflationary attractors, *J. Cosmol. Astropart. Phys.* **10** (2013) 033.
- [88] R. Kallosh and A. Linde, Multi-field conformal cosmological attractors, *J. Cosmol. Astropart. Phys.* **12** (2013) 006.
- [89] R. Kallosh, A. Linde, and D. Roest, Universal attractor for inflation at strong coupling, *Phys. Rev. Lett.* **112**, 011303 (2014).
- [90] R. Kallosh, A. Linde, and D. Roest, Superconformal inflationary  $\alpha$ -attractors, *J. High Energy Phys.* **11** (2013) 198.
- [91] M. Galante, R. Kallosh, A. Linde, and D. Roest, Unity of cosmological inflation attractors, *Phys. Rev. Lett.* **114**, 141302 (2015).
- [92] R. Kallosh and A. Linde, Polynomial  $\alpha$ -attractors, *J. Cosmol. Astropart. Phys.* **04** (2022) 017.
- [93] L. Iacconi, H. Assadullahi, M. Fasiello, and D. Wands, Revisiting small-scale fluctuations in  $\alpha$ -attractor models of inflation, *J. Cosmol. Astropart. Phys.* **06** (2022) 007.
- [94] D. Frolovsky, S. V. Ketov, and S. Saburov, E-models of inflation and primordial black holes, *Front. Phys.* **10**, 1005333 (2022).
- [95] D. Frolovsky and S. V. Ketov, Production of primordial black holes in improved E-models of inflation, *Universe* **9**, 294 (2023).
- [96] G. R. Dvali and S. H. H. Tye, Brane inflation, *Phys. Lett. B* **450**, 72 (1999).
- [97] C. P. Burgess, M. Majumdar, D. Nolte, F. Quevedo, G. Rajesh, and R.-J. Zhang, The inflationary brane anti-brane universe, *J. High Energy Phys.* **07** (2001) 047.
- [98] L. Lorenz, J. Martin, and C. Ringeval, Brane inflation and the WMAP data: A Bayesian analysis, *J. Cosmol. Astropart. Phys.* **04** (2008) 001.
- [99] R. Kallosh, A. Linde, and Y. Yamada, Planck 2018 and brane inflation revisited, *J. High Energy Phys.* **01** (2019) 008.
- [100] M. Braglia, A. Linde, R. Kallosh, and F. Finelli, Hybrid  $\alpha$ -attractors, primordial black holes and gravitational wave backgrounds, *J. Cosmol. Astropart. Phys.* **04** (2023) 033.
- [101] R. Saito, J. Yokoyama, and R. Nagata, Single-field inflation, anomalous enhancement of superhorizon fluctuations, and non-Gaussianity in primordial black hole formation, *J. Cosmol. Astropart. Phys.* **06** (2008) 024.
- [102] G. Franciolini, A. Kehagias, S. Matarrese, and A. Riotto, Primordial black holes from inflation and non-Gaussianity, *J. Cosmol. Astropart. Phys.* **03** (2018) 016.
- [103] R.-G. Cai, S. Pi, and M. Sasaki, Gravitational waves induced by non-Gaussian scalar perturbations, *Phys. Rev. Lett.* **122**, 201101 (2019).
- [104] A. Kehagias, I. Musco, and A. Riotto, Non-Gaussian formation of primordial black holes: Effects on the threshold, *J. Cosmol. Astropart. Phys.* **12** (2019) 029.
- [105] V. Atal and C. Germani, The role of non-Gaussianities in primordial black hole formation, *Phys. Dark Universe* **24**, 100275 (2019).
- [106] F. Ricciardi, M. Taoso, and A. Urbano, Solving peak theory in the presence of local non-Gaussianities, *J. Cosmol. Astropart. Phys.* **08** (2021) 060.
- [107] F. Zhang, Y. Gong, J. Lin, Y. Lu, and Z. Yi, Primordial non-Gaussianity from G-inflation, *J. Cosmol. Astropart. Phys.* **04** (2021) 045.
- [108] F. Zhang, J. Lin, and Y. Lu, Double-peaked inflation model: Scalar induced gravitational waves and primordial-black-hole suppression from primordial non-Gaussianity, *Phys. Rev. D* **104**, 063515 (2021); **104**, 129902(E) (2021).
- [109] Q. Gao, Y. Gong, and Z. Yi, Primordial black holes and secondary gravitational waves from natural inflation, *Nucl. Phys.* **969B**, 115480 (2021).
- [110] Q. Gao, Primordial black holes and secondary gravitational waves from chaotic inflation, *Sci. China Phys. Mech. Astron.* **64**, 280411 (2021).
- [111] J. S. Bullock and J. R. Primack, Non-Gaussian fluctuations and primordial black holes from inflation, *Phys. Rev. D* **55**, 7423 (1997).
- [112] P. Ivanov, Nonlinear metric perturbations and production of primordial black holes, *Phys. Rev. D* **57**, 7145 (1998).

- [113] J. Yokoyama, Cosmological constraints on primordial black holes produced in the near critical gravitational collapse, *Phys. Rev. D* **58**, 107502 (1998).
- [114] G. Ferrante, G. Franciolini, A. Junior Iovino, and A. Urbano, Primordial non-Gaussianity up to all orders: Theoretical aspects and implications for primordial black hole models, *Phys. Rev. D* **107**, 043520 (2023).
- [115] V. Atal and G. Domènech, Probing non-Gaussianities with the high frequency tail of induced gravitational waves, *J. Cosmol. Astropart. Phys.* **06** (2021) 001; **10** (2023) E01.
- [116] S. Choudhury, A. Karde, S. Panda, and M. Sami, Primordial non-Gaussianity from ultra slow-roll Galileon inflation, *J. Cosmol. Astropart. Phys.* **01** (2024) 012.
- [117] S. Choudhury, K. Dey, A. Karde, S. Panda, and M. Sami, Primordial non-Gaussianity as a saviour for PBH overproduction in SIGWs generated by pulsar timing arrays for Galileon inflation, [arXiv:2310.11034](https://arxiv.org/abs/2310.11034).
- [118] C. T. Byrnes, E. J. Copeland, and A. M. Green, Primordial black holes as a tool for constraining non-Gaussianity, *Phys. Rev. D* **86**, 043512 (2012).
- [119] G. Agazie *et al.* (NANOGrav Collaboration), The NANOGrav 15 yr data set: Detector characterization and noise budget, *Astrophys. J. Lett.* **951**, L10 (2023).
- [120] J. Antoniadis *et al.* (EPTA and InPTA Collaborations), The second data release from the European pulsar timing array—III. Search for gravitational wave signals, *Astron. Astrophys.* **678**, A50 (2023).
- [121] K. N. Abazajian *et al.* (CMB-S4 Collaboration), CMB-S4 science book, first edition, [arXiv:1610.02743](https://arxiv.org/abs/1610.02743).
- [122] T. Matsumura *et al.*, Mission design of LiteBIRD, *J. Low Temp. Phys.* **176**, 733 (2014).
- [123] K. Inomata and T. Nakama, Gravitational waves induced by scalar perturbations as probes of the small-scale primordial spectrum, *Phys. Rev. D* **99**, 043511 (2019).
- [124] K. Inomata, M. Kawasaki, and Y. Tada, Revisiting constraints on small scale perturbations from big-bang nucleosynthesis, *Phys. Rev. D* **94**, 043527 (2016).
- [125] D. J. Fixsen, E. S. Cheng, J. M. Gales, J. C. Mather, R. A. Shafer, and E. L. Wright, The cosmic microwave background spectrum from the full COBE FIRAS data set, *Astrophys. J.* **473**, 576 (1996).
- [126] S. Young, C. T. Byrnes, and M. Sasaki, Calculating the mass fraction of primordial black holes, *J. Cosmol. Astropart. Phys.* **07** (2014) 045.
- [127] I. Musco and J. C. Miller, Primordial black hole formation in the early Universe: Critical behaviour and self-similarity, *Classical Quantum Gravity* **30**, 145009 (2013).
- [128] T. Harada, C.-M. Yoo, and K. Kohri, Threshold of primordial black hole formation, *Phys. Rev. D* **88**, 084051 (2013); **89**, 029903(E) (2014).
- [129] Y. Tada and S. Yokoyama, Primordial black hole tower: Dark matter, Earth-mass, and LIGO black holes, *Phys. Rev. D* **100**, 023537 (2019).
- [130] A. Escrivà, C. Germani, and R. K. Sheth, Universal threshold for primordial black hole formation, *Phys. Rev. D* **101**, 044022 (2020).
- [131] C.-M. Yoo, T. Harada, and H. Okawa, Threshold of primordial black hole formation in nonspherical collapse, *Phys. Rev. D* **102**, 043526 (2020); **107**, 049901(E) (2023).
- [132] B. J. Carr, K. Kohri, Y. Sendouda, and J. Yokoyama, New cosmological constraints on primordial black holes, *Phys. Rev. D* **81**, 104019 (2010).
- [133] B. Dasgupta, R. Laha, and A. Ray, Neutrino and positron constraints on spinning primordial black hole dark matter, *Phys. Rev. Lett.* **125**, 101101 (2020).
- [134] H. Niikura *et al.*, Microlensing constraints on primordial black holes with Subaru/HSC Andromeda observations, *Nat. Astron.* **3**, 524 (2019).
- [135] K. Griest, A. M. Cieplak, and M. J. Lehner, New limits on primordial black hole dark matter from an analysis of Kepler source microlensing data, *Phys. Rev. Lett.* **111**, 181302 (2013).
- [136] P. Tisserand *et al.* (EROS-2 Collaboration), Limits on the macho content of the galactic halo from the EROS-2 survey of the magellanic clouds, *Astron. Astrophys.* **469**, 387 (2007).
- [137] V. Poulin, P. D. Serpico, F. Calore, S. Clesse, and K. Kohri, CMB bounds on disk-accreting massive primordial black holes, *Phys. Rev. D* **96**, 083524 (2017).
- [138] C. J. Moore, R. H. Cole, and C. P. L. Berry, Gravitational-wave sensitivity curves, *Classical Quantum Gravity* **32**, 015014 (2015).
- [139] J. Luo *et al.* (TianQin Collaboration), TianQin: A spaceborne gravitational wave detector, *Classical Quantum Gravity* **33**, 035010 (2016).
- [140] P. Amaro-Seoane *et al.* (LISA Collaboration), Laser interferometer space antenna, [arXiv:1702.00786](https://arxiv.org/abs/1702.00786).
- [141] W.-R. Hu and Y.-L. Wu, The Taiji program in space for gravitational wave physics and the nature of gravity, *Natl. Sci. Rev.* **4**, 685 (2017).
- [142] C. T. Byrnes, M. Gerstenlauer, S. Nurmi, G. Tasinato, and D. Wands, Scale-dependent non-Gaussianity probes inflationary physics, *J. Cosmol. Astropart. Phys.* **10** (2010) 004.
- [143] P. A. R. Ade *et al.* (Planck Collaboration), Planck 2015 results. XVII. Constraints on primordial non-Gaussianity, *Astron. Astrophys.* **594**, A17 (2016).
- [144] D. K. Hazra, L. Sriramkumar, and J. Martin, BINGO: A code for the efficient computation of the scalar bi-spectrum, *J. Cosmol. Astropart. Phys.* **05** (2013) 026.
- [145] J. M. Maldacena, Non-Gaussian features of primordial fluctuations in single field inflationary models, *J. High Energy Phys.* **05** (2003) 013.
- [146] P. Creminelli and M. Zaldarriaga, Single field consistency relation for the 3-point function, *J. Cosmol. Astropart. Phys.* **10** (2004) 006.